Preliminary EPR study of a solid-solid critical point in CaCO₃ near 200 °C and 1.5 GPa

J. Dean Barnett and H. Mark Nelson

Department of Physics and Astronomy, Brigham Young University, Provo, Utah 84602

(Received 9 September 1985)

EPR measurements at modestly elevated temperatures near the calcite $CaCO_3(II)$ phase line indicate the existence of critical phenomena near 200 °C and 1.5 GPa. Experimental EPR line shifts exhibit power-law variation with temperature and pressure. The EPR shifts are related to an order parameter through a microscopic model. This analysis yields an unusual critical exponent for the order parameter of approximately $\frac{1}{8}$. The model calculations involve a single condensed soft mode described by a linear combination of ten normal modes. With the assumption of a rigid CO_3 ion, there are only five unique coefficients in the linear combination, and these coefficients can be evaluated from the EPR data.

I. INTRODUCTION

In a previous paper,[1] hereafter referred to as paper I, we reported EPR data for the $CaCO_3(II)$ phase of $CaCO_3$ at pressures above the displacive first-order transition near 1.6 GPa at room temperature. We interpreted these data using a spin Hamiltonian for the Mn^{2+} impurity ion at the calcium site, which has a point-group symmetry of one (no symmetry), of the form

$$\mathscr{H} = (\mathbf{H} \cdot \overset{\leftrightarrow}{\mathbf{g}} \cdot \mathbf{S}) + A\mathbf{I} \cdot \mathbf{S} + B_{20}O_{20} + B_{22}O_{22}$$
$$+ B_{40}O_{40} + B'_{43}O'_{43} \ . \tag{1}$$

The $B'_{43}O'_{43}$ term is related to a coordinate axis of the Ca site in calcite, and the unprimed terms are related to the effective principal axes for the crystal field at the site defined by the dominant B_{20} and B_{22} terms themselves. We reported the effective site axes to be reoriented from the calcite crystal lattice axes by Eulerian angles of $\pm 30°$, $\pm 17°$, and $\pm 30°$. We also reported a significant variation of the B_{20}, B_{22}, and tilt angle θ (17°) with pressure.

The purpose of this paper is first to report some preliminary experimental data at elevated temperature that give strong evidence for the existence of some type of a solid-solid critical point along the calcite-$CaCO_3(II)$ phase line at approximately 200 °C and 1.5 GPa. Second, we want to report the calculations of the local electrostatic potential variations associated with the atomic displacements in a microscopic model. The model assumes a symmetry break and a continuous phase transition at the critical point, with atomic displacements from the high-symmetry positions that are consistent with a condensed soft mode. The comparison of these calculations with our preliminary data allows us to interpret the observed variations in the EPR data in terms of atomic displacements within the crystal. This analysis also enables us to determine a critical exponent associated with the order parameter for the continuous transition.

II. STUDY OF VARIATIONS WITH TEMPERATURE

We initiated a preliminary investigation of the EPR pattern of $CaCO_3(II)$ at moderately elevated temperatures

and varying pressure for the following two reasons. First, the significant variations of $CaCO_3(II)$ EPR pattern with pressure imply motion of the equilibrium atomic positional parameters at pressures above the transformation, and this motion in turn suggests precursors to the phase transformation from the high-pressure low-symmetry side. Second, the phase line for the calcite-$CaCO_3(II)$ transition measured using ultrasonic techniques up to 600 °C by Kondo *et al.*[2] and illustrated in Fig. 1 shows a marked curvature, which is anomalous for solid-solid phase lines.

As indicated in Fig. 1, we took measurements along the two paths, A and B, of the $+\frac{5}{2} \rightarrow +\frac{3}{2}$ resonant line position with **H** parallel to the y axis of the crystal field site and of the $-\frac{3}{2} \rightarrow -\frac{5}{2}$ line position with **H** parallel to the z axis of the crystal-field site. We also monitored the orientation of the y_1 and z_1 axes relative to the original calcite lattice axis. (Orientation of axes are specified in paper I.) The measured line position of the $+\frac{5}{2} \rightarrow +\frac{3}{2}$
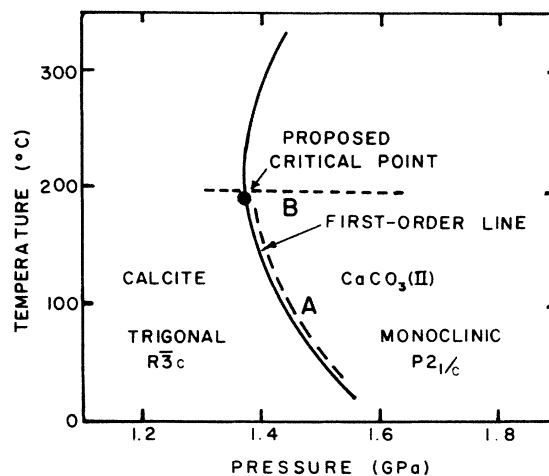

FIG. 1. Pertinent phase diagram of $CaCO_3$ showing lines A and B along which preliminary EPR data were taken, which data suggest an approach to a continuous transition at a proposed critical point.

transition in the y_1 direction as a function of temperature along path A and as a function of pressure along path B is shown in Fig. 2. The high sensitivity of the line positions to both temperature and pressure in the region of 1.5 GPa and 180 °C and the very shape of the variation suggest the existence of a critical region. The data along path A were taken by decreasing pressure and recording the line position just prior to the transition. These data thus represent direct measurements of the microscopic discontinuity between the calcite and the $CaCO_3(II)$ structures along the phase line. The fact that a discontinuity associated with a first-order phase transition is approaching zero suggests the existence of a critical point, and the fact that at tem-

peratures above this point there is critical behavior as one leaves the phase line lends further support to this suggestion. The report by Matsushima et al.[3] of a high ultrasonic loss factor in the region close to the proposed critical point is consistent with this proposal.

From the data of Fig. 2, the shift in the resonance H does not actually get very close to zero but instead shows an approach and then a discontinuity. One must ask if this discontinuity is an experimental limitation or a characteristic of the material. The study of critical phenomena requires pressure and temperature precision and control significantly better than that available in the present preliminary study. Work to provide this capability is now under way. Since variations near critical points obey critical exponent relationships, log-log plots of the data in Fig. 2 are shown in Fig. 3. These log-log plots yield expressions of the form

$$(H - H_0) = a(T - T_0)^{1/4} \tag{2a}$$

and

$$(H - H_0) = a'(P - P_0)^{1/4} . \tag{2b}$$

The one-fourth power variation of ΔH with pressure and temperature illustrates the severe requirements placed on pressure and temperature control apparatus in order to make meaningful measurements. The apparatus used was surely not adequate. We note that the data obtained are consistent with a straight line on a log-log plot, suggesting a meaningful critical exponent and the possible existence
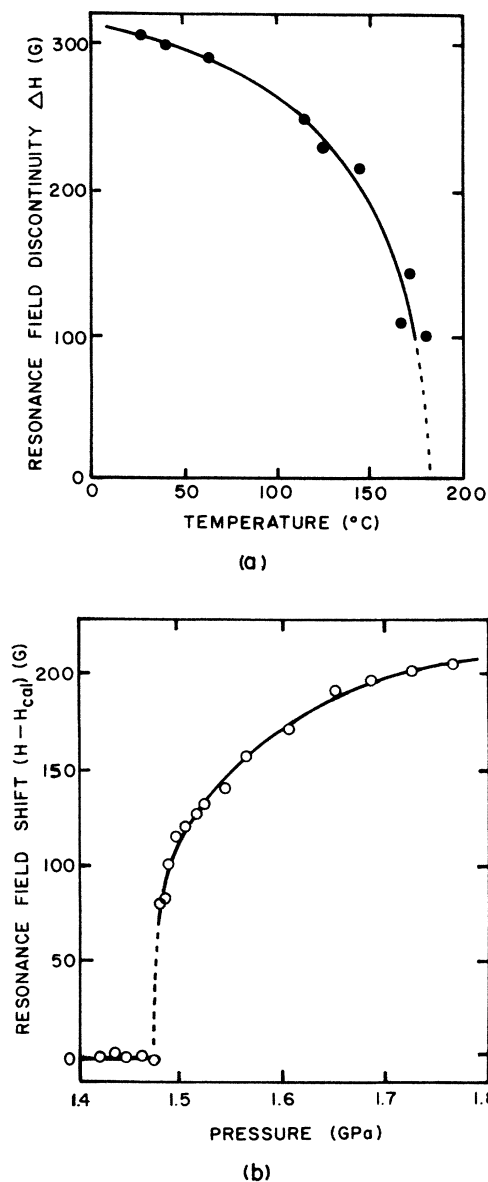

FIG. 2. (a) Discontinuity in the resonance line ($\frac{5}{2} \rightarrow \frac{3}{2}$) position across the first-order phase transition along path A of Fig. 1 as a function of temperature. (b) Shift of the resonance line ($\frac{5}{2} \rightarrow \frac{3}{2}$) from the calcite position along path B of Fig. 1 as a function of pressure.
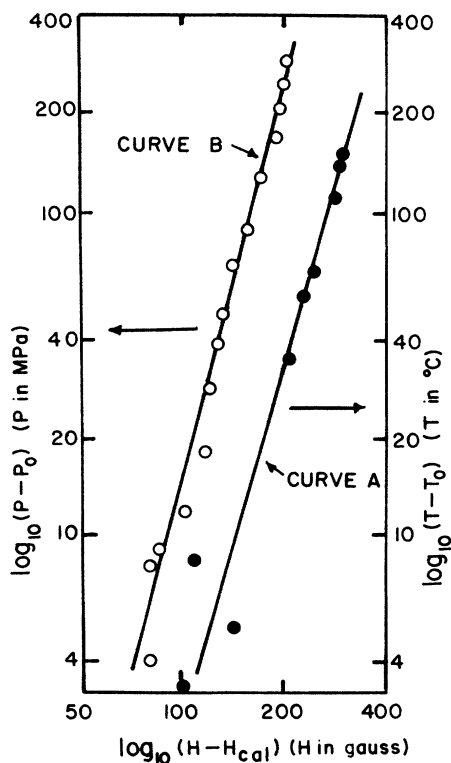

FIG. 3. Log-log plots of data given in Fig. 2 showing the power-law character of this data.

of a critical point. Thus the discontinuity observed near the critical point is very possibly a result of experimental limitations. This result is, of course, only postulatory and there may be an approach to criticality followed by a first-order phase change.

In addition to the shift in resonant line position, the change in orientation of the principal axes of the crystal field (as defined in paper I) was observed along paths A and B. Although the data were not quantitatively recorded with sufficient care to be reported, the crystal-field axes approach the calcite axes with θ decreasing from 17° ($z_1 \rightarrow z$, while y_1 approaches an axis rotated 60° from y). See Fig. 2 in paper I.

III. MICROSCOPIC MODEL

We calculated the electrostatic potential at the Mn^{2+} impurity site through a lattice sum for atomic positions consistent with a condensed soft mode. The symmetry of the soft mode suggests possible static atomic displacements from the positions in the high-symmetry calcite phase, but due to the relatively low symmetry of this particular mode, ten independently specified positional parameters are required. The assumption of a rigid CO_3 ion reduces this number to five parameters. A microscopic order parameter defined in terms of these positional parameters allows the calculation of the variation of the local electrostatic potential with the order parameter. These calculations in turn allow the microscopic interpretation of the EPR data.

A. Description of the model

Hatch and Merrill[4] have shown that the symmetry break from space group $R\bar{3}c$ (D_{3d}^6) to $P2_1/c$ (C_{2h}^5) associated with the calcite-$CaCO_3(II)$ transition can be described by a single irreducible representation of the $R\bar{3}c$ (D_{3d}^6) space group associated with a wave vector at the F point of the Brillouin zone. These authors have also shown that the static atomic displacements consistent with such a continuous transition must be expressible as a linear combination of ten uniquely defined coordinated displacements or symmetry vectors (or normal modes), all of which exhibit the same symmetry. The designation and description of these symmetry vectors are given in Table I where the displacements are referred to Fig. 4. In mathematical form we can write

$$\psi_{sm} = \sum_{i=1}^{10} a_i \psi_i \ , \tag{3}$$

where each a_i must be specified and the subscript sm denotes soft mode.

We make one simplifying assumption that makes the problem tractable when applied to our EPR data. Since a soft mode involves a low-energy phonon, and since the bonding within the CO_3 ion is known to be rather strong, we assume that no relative motion within the CO_3 ion is involved in the soft mode, and thus it can be considered rigid. We further note that since any displacement of the overall crystal is unimportant, we can choose any point within the $CaCO_3(II)$ structure as an origin to describe the

TABLE I. Possible symmetry vectors Ψ_i of the rhombohedral unit-cell group of $CaCO_3$ for the appropriate F point irreducible representation associated with the transition. The calcite reference axes in Fig. 1 of paper I are used to describe the atomic displacements. See Fig. 4 below.

Symmetry vector	Displacement relationship
ψ_1	$X_{Ca(1)} = X_{Ca(2)}$
ψ_2	$Y_{Ca(1)} = -Y_{Ca(2)}$
ψ_3	$Z_{Ca(1)} = Z_{Ca(2)}$
ψ_4	$X_{C(1)} = X_{C(2)}$
ψ_5	$Z_{C(1)} = Z_{C(2)}$
ψ_6	$X_{O(1)} = X_{O(2)}$
ψ_7	$Z_{O(1)} = Z_{O(2)}$
ψ_8	$Y_{O(3)} = Y_{O(4)} = -Y_{O(5)} = -Y_{O(6)}$
ψ_9	$X_{O(3)} = X_{O(4)} = X_{O(5)} = X_{O(6)}$
ψ_{10}	$Z_{O(3)} = Z_{O(4)} = Z_{O(5)} = Z_{O(6)}$

displacements given in Table I. We choose the origin at the center of mass of the rigid CO_3 ion and use the same reference coordinate axes used in paper I (Fig. 1). The following relationships are then valid:

$$a_4 = a_5 = 0; \quad a_9 = -\tfrac{1}{2}a_6; \quad a_8 = (\sqrt{3}/2)a_6; \quad a_{10} = -\tfrac{1}{2}a_7 \ . \tag{4}$$

We can then group the terms in Eq. (3) as

$$\psi_{sm} = (a_1\psi_1 + a_2\psi_2 + a_3\psi_3)$$
$$+ (a_6\psi_6 + a_8\psi_8 + a_9\psi_9) + (a_7\psi_7 + a_{10}\psi_{10})$$
$$= R_0\psi_{Ca\text{-}trans} + \eta\psi_{CO_3\text{-}rot} + \epsilon\psi_{CO_3\text{-}tilt} \ , \tag{5}$$

where $\psi_{Ca\text{-}trans}$ is a vector displacement of the calcium ion from their high-symmetry position in an arbitrary direction specified by either a_1, a_2, and a_3 or by the spherical
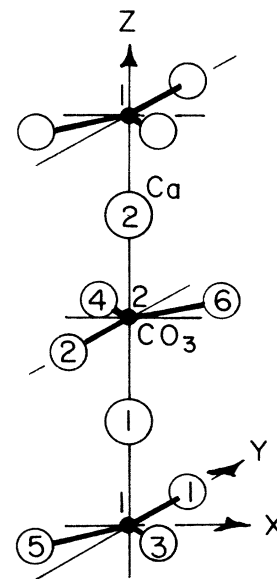

FIG. 4. Reference diagram for studying possible symmetry vectors.

coordinates $R_0 a_0$, ϕ_0, θ_0; $\psi_{CO_3\text{-rot}}$ is a rotational displacement $\eta = a_6$ of the rigid CO_3 ions about the reference z axis; and $\psi_{CO_3\text{-tilt}}$ is a rotational displacement $\epsilon = a_7$ of the CO_3 ion around the reference x axis. For convenience we have written the magnitude of the Ca-ion displacement in units of the hexagonal crystal-lattice constant a_0 so that R_0 is dimensionless and thus consistent with the dimensionless angles η and ϵ.

Our model thus consists of the coordinated displacements of point charges under the assumption of a rigid CO_3 ion with model variables R_0, ϕ_0, θ_0, η, and ϵ. We note that R_0, η, and ϵ are all zero in calcite and for a continuous transition must simultaneously approach zero as the critical point is approached from the $CaCO_3(II)$ phase. We expect this simple point-charge model to yield appropriate functional variations and symmetry features of the local potential and allow an interpretation of the associated EPR data although the quantitive features may not be totally reliable. In reality, this simple model provides greater insight than we had originally expected.

It is important to realize that our model does not require the point charges be centered on the atomic nuclei or that positional parameters determined from EPR data interpreted through this model would agree with positional parameters determined from x-ray diffraction data.

X-ray diffraction techniques locate primarily the core electrons centered about the nuclei. The local potentials calculated below for comparison with EPR data are a consequence of all charges, both positive and negative, and the effects of the spherically symmetric part of the electronic charge distribution (the core electrons) are cancelled by an equivalent amount of the nuclear charge. EPR data interpreted using our approach thus indicates the displacement of the nonspherical component of the negative charge distribution, which is essentially that associated with the valence electrons. Our model simply implies that the shifts in the valence electronic distribution from the high-symmetry charge distribution can be described by a set of "effective point charges" displaced in the same symmetry-related manner as the atomic nuclei (i.e., the soft mode).

Group theory demands the symmetry of the charge distribution of these valence-related charge displacements be precisely the same as that of the core displacements even though the magnitude of the displacement of these "effective point charges" may be significantly different from the displacement of the nuclei. Thus, the normal mode parameters discussed above for atoms and ions are used and interpreted in the EPR data as the displacement for the effective point charges.

B. Lattice sum

Since EPR data are analyzed using spin-Hamiltonian coefficients related directly to classical coefficients in the spherical harmonic expansion of the local potential and since the overwhelmingly dominant terms in the calcite and $CaCO_3(II)$ EPR data are the B_{20} and B_{22} terms, we calculate directly the coefficients of $Y_{2m}(m = 0, \pm 1, \pm 2)$ terms in the potential expansion at the Mn^{2+} site. From the well-known multipole expansion for the field of a point charge, we can write for $|\mathbf{r}|$ less than all $|\mathbf{r}_i|$

$$
\begin{aligned}
V(\mathbf{r}) &= \sum_i \frac{q_i}{4\pi\epsilon_0 |\mathbf{r} - \mathbf{r}_i|} \\
&= \sum_i \frac{q_i}{\epsilon_0} \sum_{l=0}^{\infty} \sum_{m=-l}^{+l} \frac{r^l}{(2l+1)r_i^{l+1}} Y_{lm}^*(\theta_i', \phi_i') Y_{lm}(\theta, \phi) \\
&= \sum_{l=0}^{\infty} \sum_{m=-l}^{+l} r^l A_{lm} Y_{lm}(\theta, \phi) ,
\end{aligned}
\tag{6}
$$

where

$$
A_{lm} = \frac{1}{(2l+1)\epsilon_0} \sum_i \frac{q_i}{r_i^{l+1}} Y_{lm}^*(\theta_i', \phi_i')
$$

and where i runs over all atoms considered. Since the complex coefficients A_{lm} for corresponding positive and negative m values are related, it is necessary to calculate both the real (R) and imaginary (I) parts of only the positive m values. We calculated A_{20}, $A_{2m}(R)$, and $A_{2m}(I)$ for $m = 1,2$. We placed charges on all atomic sites that lie within a large rhombohedral "cell" that is symmetrically distributed around the local Mn^{2+} impurity site. We placed whole charges at atomic sites within the cell and assigned fractional charges at the border of the cell in the spirit of the Evjen method of calculating lattice sums to obtain a rapidly converging series. The first cell included 32 molecules; a second and third layer expanded the size of the region to 27 times and 125 times larger in volume, respectively. The A_{2m} coefficients for the calculations including the second and third regions agreed with each other to within less than 0.1%, so only the second sized cell was used in most calculations. The origin for the potential function was placed on the site of the Mn^{2+} ion, which we assumed to move as if it were a Ca atom.

C. Relationship between symmetry vector coefficients

In the situation where a single soft mode drives the transition and the symmetry vector of the mode is composed of a linear combination of basis symmetry vectors, the theory of continuous phase transitions demands that a single order parameter exhibit the dominant variation when one is very near the transition. This condition implies that all ratios of coefficients a_i in the linear combination forming the soft-mode symmetry vector given in Eq. (3) be constant (independent of the order parameter). The ratios given in Eq. (4) above are consistent with this condition. Thus, near the transition we expect $R_0/\eta = D$ (a constant) and $\epsilon/\eta = E$ (a constant). Furthermore, the angles ϕ_0 and θ_0 should be independent of the order parameter since they involve only ratios between the coefficients a_1, a_2, and a_3,

$$
\tan\phi_0 = \frac{a_2}{a_1}, \quad \tan\theta_0 = \frac{(a_2^2 + a_1^2)^{1/2}}{a_3} .
$$

The value of the constants D, E, ϕ_0, and θ_0 cannot be determined by group-theoretical techniques but must be obtained through experimentation or force model calculations. The EPR data interpreted through the point-charge model allows evaluation of these parameters as shown

below. We also note that any one of R_0, ϵ, or η can be individually considered the microscopic order parameter for the transition.

Since at this point we are basically interested in the features of our data that suggest the existence of critical phenomena and a continuous phase transition near which η, ϵ, and R_0 will all be small, we calculate the A_{2m} coefficients for several values of η and ϵ (up to 1°) and R_0 up to 0.05 and for a range of θ_0 and ϕ_0 values. To simplify notation, we define a difference

$$\Delta A_{20} = [A_{20}(\eta,\epsilon,R_0,\phi_0,\theta_0) - A_{20}(0,0,0,\phi_0,\theta_0)]$$

and let $\Delta A_{20} = A_0$, $A_{21}(I) = A_1$, $A_{21}(R) = A_2$, $A_{22}(I) = A_3$, and $A_{22}(R) = A_4$. Empirical equations fit to the results of these A_{lm} calculations demonstrate that the five A_n coefficients each exhibit variations with η, ϵ, and R_0 of a generalized quadratic form

$$A_n = a_{n1}R_0^2 + a_{n2}\epsilon^2 + a_{n3}R_0\epsilon$$
$$+ a_{n4}\eta R_0 + a_{n5}\eta\epsilon + a_{n6}\eta^2 \quad (n=0,\ldots,4) \quad (7)$$

for any chosen pair of θ_0 and ϕ_0. The coefficients $a_{16} = a_{26} = a_{36} = a_{46} = a_{05}$ were zero for all θ_0 and ϕ_0 pairs. Thus, we conclude that the 25 nonzero coefficients a_{nj} are each functions of θ_0 and ϕ_0 only. Furthermore, since $R_0 = D\eta$ and $\epsilon = E\eta$, Eq. (7) could be written as

$$A_n = \eta^2(a_{n1}D^2 + a_{n2}E^2 + a_{n3}DE + a_{n4}D + a_{n5}E + a_{n6})$$
$$= \eta^2 G_n(\theta_0,\phi_0) . \quad (7')$$

Thus, for every θ_0 and ϕ_0 pair, each A_n varies with the square of the order parameter, and ratios of any two A_n values will be independent of η.

D. Transformation of calculated coefficients to site axes

Our experimental EPR data are analyzed with reference to the crystal-field site axes defined by the $B_{22}O_{22}$ and $B_{20}O_{20}$ terms in the Hamiltonian as described in paper I, whereas our calculations are made relative to the fixed reference axes of the calcite lattice. We must thus transform our calculated results to rotated axes for comparison with the data. The data are condensed into five uniquely significant values: the difference $\Delta B_{20} = [B_{20}(\text{phase II}) - B_{20}(\text{calcite})]$, B_{22}, and the three Eulerian angles (ϕ,θ,ψ) that orient the principal axes of the crystal field relative to the calcite lattice axes. We have limited data on the variation of these five parameters with temperature and pressure. Specifically, ϕ and ψ do not vary, B_{22} varies as $(T-T_0)^{1/4}$ and $(P-P_0)^{1/4}$, and θ varies approximately like B_{22}.

In order to find the proper angles to rotate the axes of our calculated potential function to fit a site axes, we realize that any potential associated with the sum of the five spherical harmonics with $l=2$ is a quadratic form in Cartesian coordinates. In equation form,

$$V(x,y,z) = \sum_{m=-2}^{+2} A_{2m}r^2 V_{2m} = \sum_{i=1}^{3}\sum_{j=1}^{3} c_{ij}x_ix_j . \quad (8)$$

The principal axes can be readily determined by standard eigenvalue techniques, in which the eigenvectors point along the principal axes. When the potential is described with respect to these rotated principal axes, only the $A_{20}Y_{20}$ and $A_{22}Y_{22}$ terms will appear in the spherical harmonic potential expansion. This eigenvalue problem involves a cubic equation and can be simply solved to obtain algebraic expressions for the eigenvectors under the assumption that all $A_{2m}(R/I)$ terms vary only as η^2 (near the critical point). The unnormalized rotation matrix (eigenvectors as rows) is

$$\begin{bmatrix} a & \pm a\left[\dfrac{1}{\tan(\alpha/2)}\right] & a\left[\dfrac{-2}{\sqrt{6}A_{20}}\dfrac{\sin[\beta-(\alpha/2)]}{\sin(\alpha/2)}\right] \\ b & \mp b\left[\tan\dfrac{\alpha}{2}\right] & b\left[\dfrac{2}{\sqrt{6}A_{20}}\dfrac{\cos[\beta-(\alpha/2)]}{\cos(\alpha/2)}\right] \\ c\left[\dfrac{-2}{\sqrt{6}}\dfrac{|A_{21}|}{A_{20}}\right]\cos\beta & c\left[\dfrac{2}{\sqrt{6}}\dfrac{|A_{21}|}{A_{20}}\right]\sin\beta & c \end{bmatrix}, \quad (9)$$

where

$$\tan\beta = \frac{A_{21}(I)}{A_{21}(R)} = \frac{A_1}{A_2}$$

and

$$\tan\alpha = \frac{A_{22}(I)}{A_{22}(R)} = \frac{A_3}{A_4} .$$

The presence of the $\pm$ signs is a consequence of the lack

of uniqueness in specifying which eigenvalue is associated with the x' and y' axes of the rotated system.

The required Eulerian angles that provide such a rotation matrix are easily identified by comparing this matrix with a standard matrix in terms of Eulerian angles. The parameters $A_{2m}(R/I)$ calculated from the microscopic model in the reference frame tied to the hexagonal crystal can now be related to the parameters A'_{22} and A'_{20} in the rotated system and the required Eulerian angles (ϕ',θ',ψ'). Therefore,

$$\tan\phi' = \frac{1}{\tan\beta} = \frac{A_{21}(R)}{A_{21}(I)} \; ;$$

$$\tan2(\Psi' + \phi') = \pm\tan\alpha = \pm\frac{A_{22}(I)}{A_{22}(R)} \; ; \tag{10}$$

$$\sin\theta' = \pm\frac{2}{\sqrt{6}}\frac{|A_{21}|}{A_{20}}; \quad A_{22}'(R) = |A_{22}|, \quad \text{and} \quad A_{20}' = A_{20} \; .$$

The experimental values B_{20}, B_{22}, ϕ, θ, and ψ are then assumed to correspond to the calculated value A_{20}', A_{22}', ϕ', θ', and ψ'.

We can draw two significant conclusions that relate to the experimental data in terms of functional forms and are thus expected to be valid. (1) $\sin\theta$, as well as ΔB_{20} and B_{22}, should be proportional to η^2. (2) Both the Eulerian angles ϕ and Ψ, which are determined by ratios of two A_n, depend only on ϕ_0, θ_0, D, and E and are thus theoretically independent of the order parameter. Our data which demonstrate constant ϕ and Ψ, thus appear to be consistent through this point-charge analysis with the theory of a continuous phase transformation exhibiting a single soft mode; since the theory requires constant ratios (ϕ_0, θ_0, D, E) of the coefficients in the linear combination of symmetry vectors outlined in Sec. III A above.

E. Coefficients in soft-mode linear combination

We desire to evaluate the model parameters R_0, ϕ_0, θ_0, ϵ, and η using the measured values of ϕ, θ, ψ, B_{22}, and ΔB_{20}. Although our present data is not sufficiently precise to utilize the results of this analysis in a meaningful way, we present the analysis in the spirit of completeness and in anticipation of more precise data. From the EPR data in the critical region, we extract five experimental numbers:

$$N_1 = \tan\phi, \quad N_2 = \pm\tan2(\psi + \phi) \; ,$$

$$N_3 = \left|\frac{B_{22}}{B_{20}\sin\theta}\right|^2, \quad N_4 = \left|\frac{B_{22}}{\Delta B_{20}}\right|^2, \quad \text{and} \quad N_5 = \left|\frac{\Delta B_{20}}{B_{20}}\right| \; .$$

These are all ratios of spin-Hamiltonian parameters and thus can be compared with reasonable confidence to corresponding classical theoretically calculated model related ratios of the A_{lm} coefficients as presented in Eqs. (10). We can thus write

$$N_1 = \frac{A_2}{A_1} \; ; \tag{11a}$$

$$N_2 = \pm\frac{A_3}{A_4} \; ; \tag{11b}$$

$$N_3 = \frac{(A_3^2 + A_4^2)}{(A_1^2 + A_2^2)} \; ; \tag{11c}$$

$$N_4 = \frac{(A_3^2 + A_4^2)}{(A_0^2)} \; ; \tag{11d}$$

$$N_5 = \frac{A_0}{A_{20}} \; , \tag{11e}$$

where the only η variation is in Eq. (11e).

By utilizing the quadratic forms of Eq. (7), we can isolate, explicitly, the algebraic involvement of the parameters η, D, and E. We then recognize that the (θ_0, ϕ_0) variation is hidden in the a_{nj} coefficients. Equations (11a) and (11b) are general quadratic relationships in the variables D and E and involve ϕ_0 and θ_0 only through the a_{nj} coefficients. For a given pair of values for ϕ_0 and θ_0, these two quadratic forms can be solved algebraically for D and E. In general, there is a possibility of eight different solutions. For each possible solution we substitute these values of D and E into Eqs. (11c) and (11d) and obtain two functions, $P(\phi_0, \theta_0) = (A_1^2 + A_2^2)N_3 - (A_3^2 + A_4^2) = 0$ and $Q(\phi_0, \theta_0) = A_0^2 N_4 - (A_3^2 + A_4^2) = 0$. We use numerical methods to find a pair ϕ_0^* and θ_0^* that simultaneously make P and Q zero and thus satisfy the four relationships (11a)–(11d). We then easily calculate corresponding values of D^* and E^*. For any given pressure and temperature a value of η^* can then be determined. The "starred" values represent a possible "fit" of the model to the experimental results.

Our preliminary data define quite uniquely the numerical value N_1 and the numerical magnitude of N_2 with accuracy of a few percent. The quantities N_3, N_4, and N_5 are not so well known since extensive data have not been taken in the critical region; thus, only crude estimates can be made. The quantity N_5, of course, varies as the square of the order parameter and is highly pressure and temperature dependent. The other four quantities should be uniquely defined when within the critical region.

The numerical search for possible fits of the model to the data was made using both $\pm$ signs for N_2 over the total (θ_0, ϕ_0) angular quadrant within which the high-pressure x-ray data place the Ca ion. No reasonable solutions were found with N_2 positive. With N_2 negative, several extraneous solutions that required negative R_0 values (implying θ_0, ϕ_0 in a different quadrant) were discarded. There do exist well-behaved, meaningful solutions with N_2 negative when N_3 and N_4 have values within the range of our experimental estimates of N_3 and N_4. Table II indicates the general range over which D, E, ϕ_0, and θ_0 can vary as a result of the present experimental uncertainties in N_3 and N_4. For comparison, corresponding parameters taken from x-ray measurements at a point quite far removed from the critical point, are also given in Table II.

TABLE II. The range of EPR input data values and the range of model parameters determined from EPR data as interpreted through the point-charge model. The model parameters determined from x-ray data taken at room temperature (far from the critical region) are also shown for comparison. Input data: $N_1 = -\sqrt{3}$, $N_2 = -\sqrt{3}$, $N_3 = 0.85 \rightarrow 1.2$, $N_4 = 15 \rightarrow 600$.

EPR analysis near critical region	X-ray data[a] at room temperature and 1.8 GPa
$D^* = 0.025$	$D = 0.28$
$E^* = 0.8 - 1.2$	$E = 0$
$\phi_0^* = 160° - 190°$	$\phi_0 = 166°$
$\theta_0^* = 40° - 80°$	$\theta_0 = 68°$

[a]See Ref. 8.

We have included the above analysis to illustrate the potential use of the EPR data in investigating the critical region of the transformation and as a means of monitoring whether or not the parameters θ_0, ϕ_0, D, and E are truly independent of η.

IV. DISCUSSION AND CONCLUSIONS

Hatch and Merrill[4] and Hatch[5] have theoretically treated this transformation and indicate the transition can be continuous based on the Landau criteria. Hatch and Decker[6] further indicate that the order parameter associated with the calcite-$CaCO_3$(II) transformation is three dimensional but that only one component is nonzero if a single domain is created. Thus to first order, only one soft mode is involved in the electron density changes. This fact implies constant ratios of the a_i in Eq. (3). Our data illustrating constant Eulerian angles ϕ and ψ in the critical region are consistent with this theoretical result. From our point-charge model we have calculated $B_{22}(\eta)$, $\theta(\eta)$, and ΔB_{20} and find that for small η, these three experimental parameters should vary quadratically with η.

The data shown in Figs. 2 and 3, although preliminary in nature, suggest the possibility of a critical point and then suggests a critical exponent. Based on the analysis given above, this critical exponent would be rather unusual. For the resonant line studied, the variation of the EPR resonance field $(H - H_0)$ from the position observed in calcite is proportional to the value of B_{22}, which is proportional to η^2. Thus, the data and analysis imply that the microscopic order parameter for the transition varies with pressure and temperature as

$$\eta = b(P - P_0)^{1/8} = b'(T - T_0)^{1/8} .$$

The critical exponent associated with the order parameter must then be $\frac{1}{8}$. We have no explanation for this result but report it as a significant feature of the transformation. Felix and Hatch[7] have analyzed the transformation using renormalization-group techniques and indicate that although classically the transformation may appear continuous, such is not the case unless additional restrictions are imposed. For example, if the $CaCO_3$(II) phase were an incommensurate phase the transformation could be continuous. The value of $\frac{1}{8}$ for the critical exponent may be associated with this variance between the classical and renormalization group analysis, or indicate some uniqueness associated with an incommensurate continuous transformation. We must emphasize once more that our experimental data is not definitive on the continuous nature of the transformation. Additional experimental as

well as theoretical work needs to be done.

A few comments are in order relative to the analysis in Sec. III E. First, as discussed in Sec. III A, we do not expect agreement between the displacement from the high-symmetry equilibrium positions measured by x-ray diffraction and the location of some "effective point charge" associated with the valence-charge redistribution as seen by EPR data through our analysis. Furthermore, the x-ray data are taken at a pressure and temperature somewhat removed from the critical region. Notwithstanding the many uncertainties, some general interpretation of the results in Table II can be made. If $CaCO_3$ is basically ionic, as we have assumed, and the distortion of the core electrons is neglected, the effective charge on the Ca ion would really be located at the nucleus. Such an assumption provides the following: Angles ϕ_0 and θ_0 should agree with the x-ray displacements. The small value of $D = R_0/\eta$ obtained from the EPR data relative to the x-ray data suggests that near the critical point the rotational distortion of the valence cloud around the CO_3 group is much larger than the rotational displacements of the oxygen cores. The value of approximately 1.0 for $E = \epsilon/\eta$ implies that the tilting of the effective charge is significantly larger than the tilting of the cores. Such interpretations are not unreasonable. The large tilt angle ϵ compared with the rotation angle η may also be evidence that the assumption of a rigid CO_3 ion (in a valence cloud sense) is not reasonable.

We were hopeful that the point-charge-model calculations would shed some light on the apparent residual of 30° in the measured values for the Eulerian angles ϕ and ψ reported in paper I, but such was not the case. It is tempting to try to relate these residual angles in the data to the fact that our model simply displaces atoms slightly from a rhombohedral lattice and that the CO_3 groups are still centered on this residual lattice. We note that since the predictions of the experimentally measured quantities A_{20}, A_{22}, ϕ, θ, and ψ can be varied over extended ranges by varying the model parameters R_0, ϕ_0, θ_0, ϵ, and η on the same residual lattice, the residual 30° angles cannot be traceable to the residual rhombohedral lattice through this point-charge model. Rather, this model suggests that the residual 30° angles simply imply a special correlation between the model parameters R_0, θ_0, ϕ_0, ϵ, and η.

ACKNOWLEDGMENTS

[1]J. D. Barnett, H. M. Nelson, and S. D. Tyagi, Phys. Rev. B **31**, 1248 (1985).

[2]S. Kondo, K. Saito, and S. Matsushime, J. Earth Phys. **20**, 245 (1972).

[3]S. Matsushima, K. Saito, and S. Kondo, in *Proceedings of the 4th International Conference on High Pressure, AIRAPT, Kyoto, 1975*, edited by J. Osugi (Kawa Kita, Kyoto, 1975), pp. 383–388.

[4]D. M. Hatch and L. Merrill, Phys. Rev. B **23**, 368 (1981).

[5]D. M. Hatch, Phys. Rev. B **23**, 2346 (1981).

[6]D. M. Hatch and D. L. Decker, J. Chem. Phys. **74**, 2518 (1981).

[7]J. W. Felix and D. M. Hatch, Phys. Rev. Lett. **53**, 2425 (1984).

[8]L. Merrill and W. A. Bassett, Acta Crystallogr. B **31**, 343 (1975).